

PAPER • OPEN ACCESS

Deep reactive ion etching of cylindrical nanopores in silicon for photonic crystals

To cite this article: Melissa J Goodwin *et al* 2023 *Nanotechnology* **34** 225301

View the [article online](#) for updates and enhancements.

You may also like

- [Black silicon method X: a review on high speed and selective plasma etching of silicon with profile control: an in-depth comparison between Bosch and cryostat DRIE processes as a roadmap to next generation equipment](#)
H V Jansen, M J de Boer, S Unnikrishnan et al.
- [Assessment of STI dry etch process variability by means of dynamic time warping technique](#)
Alexey P. Milenin, BT Chan and Frederic Lazzarino
- [Nanoscale directional etching features and mechanism of HF/HNO₃ etchant](#)
Biyu Peng, Hongbo Wang and Haifeng Huang



WORLD LEADING
MOLECULAR
SPECTROSCOPY SOLUTIONS



edinst.com

Deep reactive ion etching of cylindrical nanopores in silicon for photonic crystals

Melissa J Goodwin¹ , Cornelis A M Hartevelde¹ , Meint J de Boer² and Willem L Vos¹ 

¹Complex Photonic Systems (COPS), MESA+ Institute for Nanotechnology, University of Twente, PO Box 217, 7500 AE Enschede, The Netherlands

²MESA+ Nanolab, MESA+ Institute for Nanotechnology, University of Twente, PO Box 217, 7500 AE Enschede, The Netherlands

E-mail: m.j.goodwin@utwente.nl

Received 4 November 2022, revised 19 January 2023

Accepted for publication 25 January 2023

Published 16 March 2023



Abstract

Periodic arrays of deep nanopores etched in silicon by deep reactive ion etching are desirable structures for photonic crystals and other nanostructures for silicon nanophotonics. Previous studies focused on realizing as deep as possible nanopores with as high as possible aspect ratios. The resulting nanopores suffered from structural imperfections of the nanopores, such as mask undercut, uneven and large scallops, depth dependent pore radii and tapering. Therefore, our present focus is to realize nanopores that have as cylindrical as possible shapes, in order to obtain a better comparison of nanophotonic observations with theory and simulations. To this end in our 2-step Bosch process we have improved the mask undercut, the uneven scallops, pore widening and positive tapering by optimizing a plethora of parameters such as the etch step time, capacitively coupled plasma (ion energy) and pressure. To add further degrees of control, we implemented a 3-step DREM (deposit, remove, etch, multistep) process. Optimization of the etching process results in cylindrical nanopores with a diameter in the range between 280 and 500 nm and a depth around 7 μm , corresponding to high depth-to-diameter aspect ratios between 14 and 25, that are very well suited for the realization of silicon nanophotonic structures.

Keywords: reactive ion etching, photonic crystals, silicon nanophotonics


(Some figures may appear in colour only in the online journal)

1. Introduction

Etching of nanopores in silicon is of interest in the research of micro-sieves [1], optical sensors [2], x-ray mirrors [3], photovoltaics [4], photonic crystals [5–7], and many more topics. Each application has its own requirements for what is needed from a pore, be it length, diameter, high aspect ratio, smooth walls or a particular shape such as conical or cylindrical. Depending on the required application, there are multiple strategies for etching pores in silicon, for example, wet etching [1, 3], metal assisted chemical etching [2],

electrochemical etching [4, 5] and dry etching techniques such as reactive ion etching (RIE) [1, 6, 8, 9].

Reactive ion etching (RIE) is a dry etching process which is compatible with complementary metal-oxide-semiconductor (CMOS) methods used in the semiconductor industry. RIE is often used to remove silicon from substrates in situations where metal contamination from wet etching is undesirable or in situations where wet etching would not give the required directionality [10, 9, 8, 11, 12]. RIE uses a reactive gas that reacts with the silicon to form volatile species which are pumped away, thereby removing silicon. This reaction is quasi-isotropic since the removal of silicon typically happens in all directions almost equally. Since isotropy is undesirable when creating high aspect ratio structures such as nanopores, or trenches, an extra step is needed to make the etch process anisotropic.

 Original content from this work may be used under the terms of the [Creative Commons Attribution 4.0 licence](https://creativecommons.org/licenses/by/4.0/). Any further distribution of this work must maintain attribution to the author(s) and the title of the work, journal citation and DOI.

One class of devices that requires high aspect ratio structures is photonic crystals. Photonic crystals are formed by a periodic variance of a high and low refractive index materials, such as a periodic arrangement of nanopores etched in silicon. The scale of the periodicity needs to be on the length scale of the wavelength of light for which a band gap is desired, for example the near infrared, which is of interest for telecommunications [13]. The diameter of the nanopores is chosen to obtain a low silicon to air ratio to maximize the photonic strength of the crystal [14]. Tuning the nanopore diameter and pitch of the pores allows one to control the position and width of the photonic band gap, comparable to how doping changes the electronic band gap in semiconductors. For the fabrication of both 2D [15, 16] and 3D silicon photonic crystals [5, 7], it is important to have good control over the shape, diameter, length and roughness of the side wall of the nanopores. For certain classes of photonic crystals, the etched structures must be as close to a perfect cylinder of a precise diameter as possible, that is, little to no tapering, minimal scalloping and no under etch. Previously, Woldering *et al* [17] explored the effects or deviations in diameter, tapering and pore misalignment, among others. They found that the photonic band gap is greatly affected by relatively small changes, so consistency and control in the manufacturing process is a must. To achieve such nanopores, an etching technique with a high degree of directionality and control must be used such as the Bosch process.

The Bosch process is a well known process that adds a large degree of directionality to RIE [8, 18]. The 2-step Bosch process consists of a protection step and an etching step. During the protection step a protective layer is deposited onto and inside the sample, notably on the sidewalls of the nanopores. Consequently, the sidewalls are protected from the subsequent ions and radicals. Moreover, the insulating nature of the protective layer decreases the image force that attracts ions to the sidewalls. During the subsequent etch step, the directional flux of ions removes the protective layer at the bottom of the nanopores and the ions and radicals present in the plasma etch the silicon further leading to a deeper nanopore. After each etch step, a protection step is performed to protect the newly formed silicon walls. This cycling of etch and protection steps results in the distinctive scallops characteristic of the Bosch process [11, 6, 17, 9, 19, 18, 8, 20, 21].

The etching of high aspect ratio structures using the Bosch process is an adjustment between multiple factors [20]. The etching process hinges on getting ions and radicals to the bottom of the pore to continue etching, while maintaining the integrity of the walls by reducing lateral etching. Even with a protective coating there are two factors that cause an undesired widening of the pores, namely the image force and the angular distribution of the incident ions [6, 21]. While the angular distribution of the ions can be controlled by varying the etch parameters, the image force is affected by the nature of the structure to be etched. When the ions are closer to the walls of the structure, the electrostatic image force is stronger, hence going from 1- to 2- to 3-dimensional structures, the effect of the image force increases. Therefore nanopores are more affected by image forces than trenches of the same

width, and a narrow 500 nm nanopore is more strongly affected than a wide 10 μm micropore. Moreover, as the ions transverse the nanopore, they lose energy, until they have lost so much energy that they are attracted to the walls, thus the longer the nanopore (or trench) becomes, the more ions will be lost due to collisions with the walls due to the image force.

Therefore, it is clear that deep nanopores with high aspect ratios are challenging to fabricate. The particular balance of parameters required for RIE is even dependent on the diameter of the nanopores, so the etch process should ideally be optimised for the particular nanopores that are required in the final device.

Unlike previous work [6, 22], our work does not concentrate on producing the highest aspect ratio pores possible. The reason is that ultradeep nanopores often entail imperfections in shape such as mask undercut, large scallops and tapering, that notably hamper the interpretation and modelling of observations and applications [23]. These imperfections can become more prominent when starting a process on a different etcher, or in a different lab, requiring the process to be optimized anew. In this work we focus on how the process parameters control the form and shape of the nanopores to create as ideal as possible nanopores for photonic (crystal) applications and create a framework for how to address undesirable feature in an etch process.

2. Materials and methods

2.1. Samples and infrastructure

For the testing of different etch parameters, so-called ‘easycleave’ structures were etched and analysed. Easycleave, as shown in figure 1, is a 1 cm by 2 cm piece of silicon wafer with a 50 nm thick chromium etch mask with arrays of apertures. The apertures are arranged with a 84.5° angle between the axis of the primitive lattice. This non- 90° angle ensures that cleaving along a wafer crystal plane will always cleave through some of the pores, hence the name easycleave [24]. The etch mask consists of arrays of circular apertures of 11 different diameters. For each diameter there are up to 7 arrays of different pore-to-pore pitches. Thus, the easycleave masks offers a broad range of structural parameters to critically test etching procedures and parameters.

As the etching instrument is designed for the use of 4 inch wafers, it is thus necessary to employ a carrier wafer to hold the easycleave samples. Carrier wafers (110, p-doped silicon, 4 inch, 500 nm thickness) were coated with a layer of positive photoresist (Olin OiR 908-35) that was spincoated at 4000 rpm and hard baked at 120°C for 10 min. The photoresist prevents the carrier wafer from being etched, which avoids unwanted etching phenomena from a high silicon loading [25], and also ensures the reuseability of the wafer. The easycleave samples were attached to the carrier wafers using a thin layer of fomblin oil, which is a vacuum-safe, perfluorinated polyether. Figure 2 shows a schematic of a nanopore in cross section, highlighting the important features and measurements that are made. The running depth is denoted by x , and the full depth of the nanopore from mask to

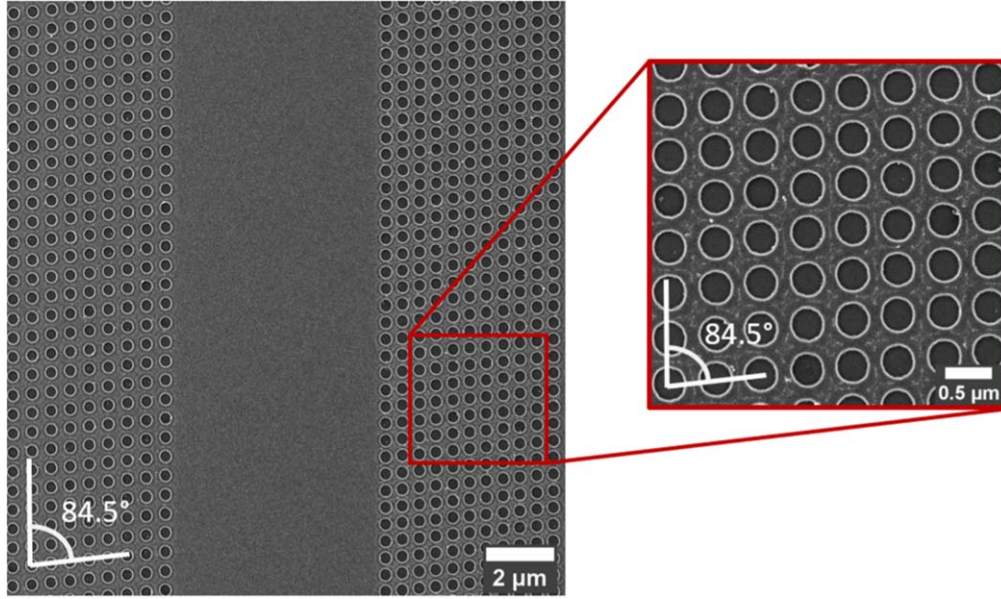


Figure 1. SEM image of an easy-cleave sample showing 320 nm diameter apertures in the chromium mask and 2 different pitches, 600 nm (left) and 500 nm (right). The 84.5° angle between the photonic crystal axes is shown. After etching the sample is cleaved along the horizontal plane in this image to reveal the cross section for SEM imaging. The inset is a higher magnification image to better show the round apertures.

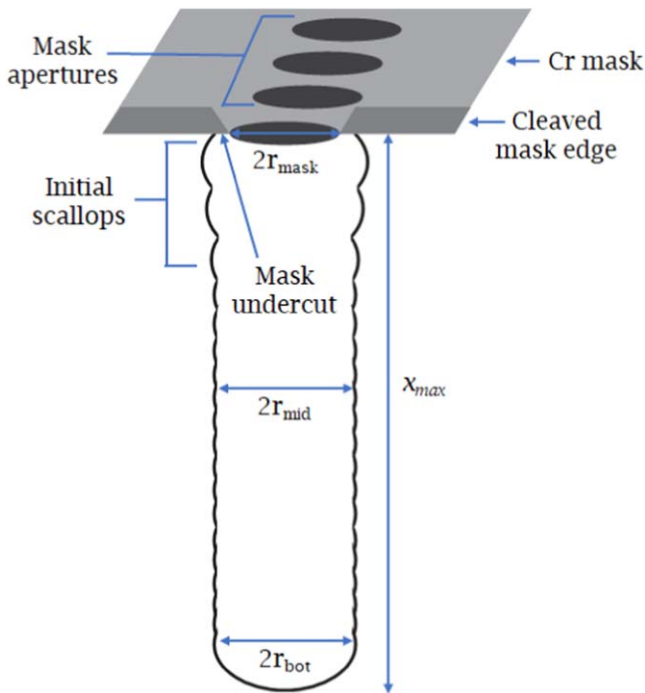


Figure 2. Schematic illustrating the main features and characteristic dimensions of a nanopore etched in silicon: x_{\max} is the maximum depth of the pore, d_{mask} the diameter of the mask aperture, d_{mid} the diameter at half depth, and d_{bot} the diameter at the bottom of the nanopore.

bottom is denoted by x_{\max} . The diameter of the mask d_{mask} is measured from cross-sectional SEM images. The mask undercut is how far under the mask the first etch step etches, determining the diameter of the nanopore. The initial scallops

are defined as the first 10 scallops of the nanopore formed in the first 10 etch cycles. The initial scallops are often more pronounced and longer than subsequent scallops. The diameter at half depth d_{mid} is taken to be the characteristic diameter of nanopore. From this diameter, we define the aspect ratio A to be

$$A \equiv \frac{x_{\max}}{d_{\text{mid}}}. \quad (1)$$

Finally, the diameter at the bottom of the pore is called d_{bot} , which gives the pore tapering angle θ that is defined as

$$\theta \equiv \arctan\left(\frac{r_{\text{top}} - r_{\text{bot}}}{x_{\max}}\right) \approx \frac{r_{\text{top}} - r_{\text{bot}}}{x_{\max}}, \quad (2)$$

where the second approximate expression in equation (2) assumes the angle to be sufficiently small to accurately approximate the trigonometric function by a low order Taylor expansion. To determine these parameters, the cross sections of the cleaved samples were imaged using scanning electron microscopy (SEM, JEOL JSM 7610F Plus FEG SEM) and the resulting images analyzed with software such as ImageJ.

2.2. Etch processes

All etching experiments were performed using a SPTS Pegasus reactive ion etcher in the MESA⁺ Nanolab using C_4F_8 as the protection gas, SF_6 as the etching gas and O_2 for plasma cleaning to remove leftover fluorocarbon from the sample surface after etching. In the protection step, a layer of insulation fluorocarbon is deposited on the substrate. In the etch step, the fluorocarbon layer is removed from the bottom of the nanopore and the silicon is etched. The steps are repeated until the desired pore length is achieved. An

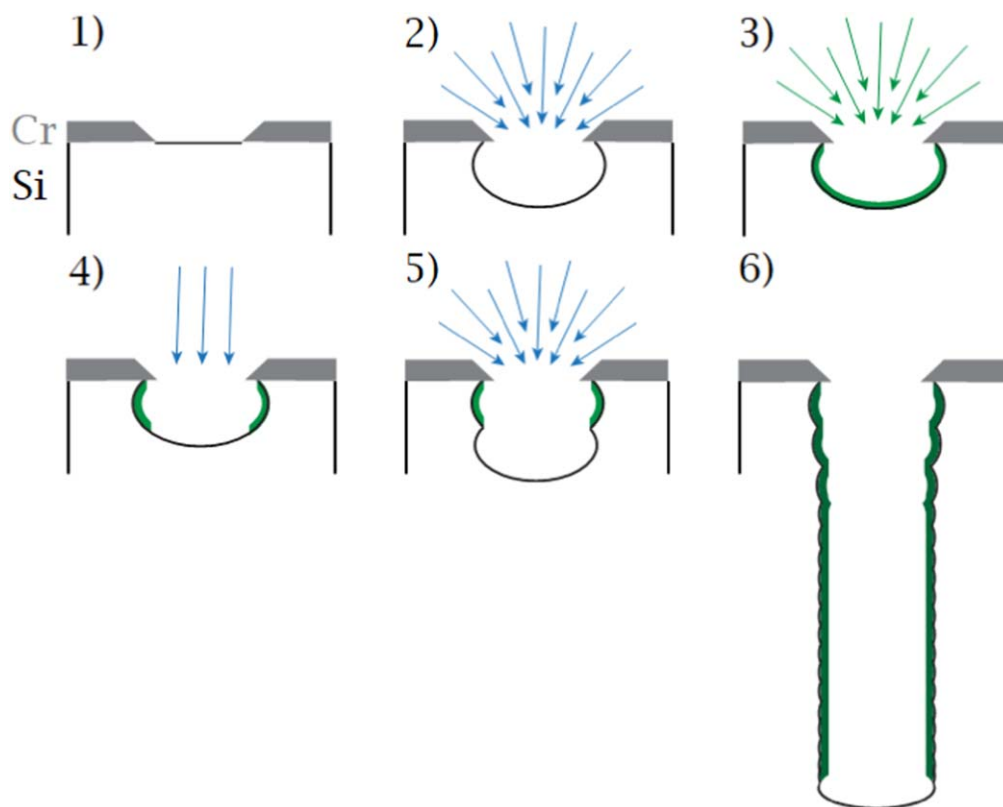


Figure 3. Schematic of the 3-step Bosch DREM process. (1) Silicon substrate with a chromium mask. (2) Isotropic etching of Si with high pressure SF_6 . (3) First named step of the 3-step process: deposition. Protection by depositing a layer of fluorocarbon using C_4F_8 . (4) Second named step: removal. Removal of the fluorocarbon layer by low pressure SF_6 with a low angular distribution. (5) Third named step: etching. Etching of Si with high pressure SF_6 with a wide angular distribution, (6) repeat deposit, remove, etch until desired pore depth.

overview of the maximum and minimum etch parameters used in this work can be found in table 1 with the full parameter list in the [appendix](#) in table 2.

Since in the 2-step process both the removal of the fluorocarbon and the etching of the silicon occur during the same etch step, only a single set of parameters is available to perform two different tasks during this step. To gain more control over the process, a 3-step Bosch process is implemented, as schematically illustrated in figure 3. The 3-step process splits the etch step into two parts, removal of fluorocarbon and etching silicon. This process is also referred to as Deposition, Removal, Etch, Multistep or DREM [19]. The removal step is performed using low pressure SF_6 . The lower pressure results in a longer mean free path for the SF_5^+ ions, resulting in less collisions and thus a greater directionality. This reduces the loss of fluorocarbon on the walls that is caused by the high angular distribution of the SF_5^+ ions [21, 26]. The low pressure also means there are fewer ions and radicals available to etch the silicon, so while some silicon will be etched during the removal step, the amount of etching should remain small due to low concentration of SF_5^+ ions and F radicals. The pressure of SF_6 is then increased for the etch step, returning to the faster, quasi-isotropic etching by ions with a wide angular distribution and radicals. The software of the SPTS Pegasus calls the fluorocarbon removal step the ‘boost step’. The boost step

Table 1. An overview of the minimum and maximum parameters used in this work. A full table of parameters can be found in the [appendix](#) in table 2.

Parameter	Unit	Minimum	Maximum
Cycles	Number	100	180
Deposition time	Seconds	1.6	1.6
Etch time	Seconds	1.5	4.0
Deposition pressure	mtorr	20	20
Etch pressure	mtorr	13	26
SF_6 flow	sccm	65	65
C_4F_8 flow	sccm	200	200
ICP frequency	MHz	13.56	13.56
ICP power deposition	Watts	1500	1500
ICP power etch	Watts	1500	1500
CCP power deposition	Watts	0	0
CCP power etch	Watts	60	90
Temperature	°C	10	10
Boost step time	Seconds	0	3
Boost throttle	Percentage	0	100

is part of the etch cycle, meaning a 3 s etch cycle with 1 s boost would be 1 s of low pressure fluorocarbon removal and 2 s of higher pressure etching. From this point on, the fluorocarbon removal step will be referred to as boost step in keeping with the SPTS software.

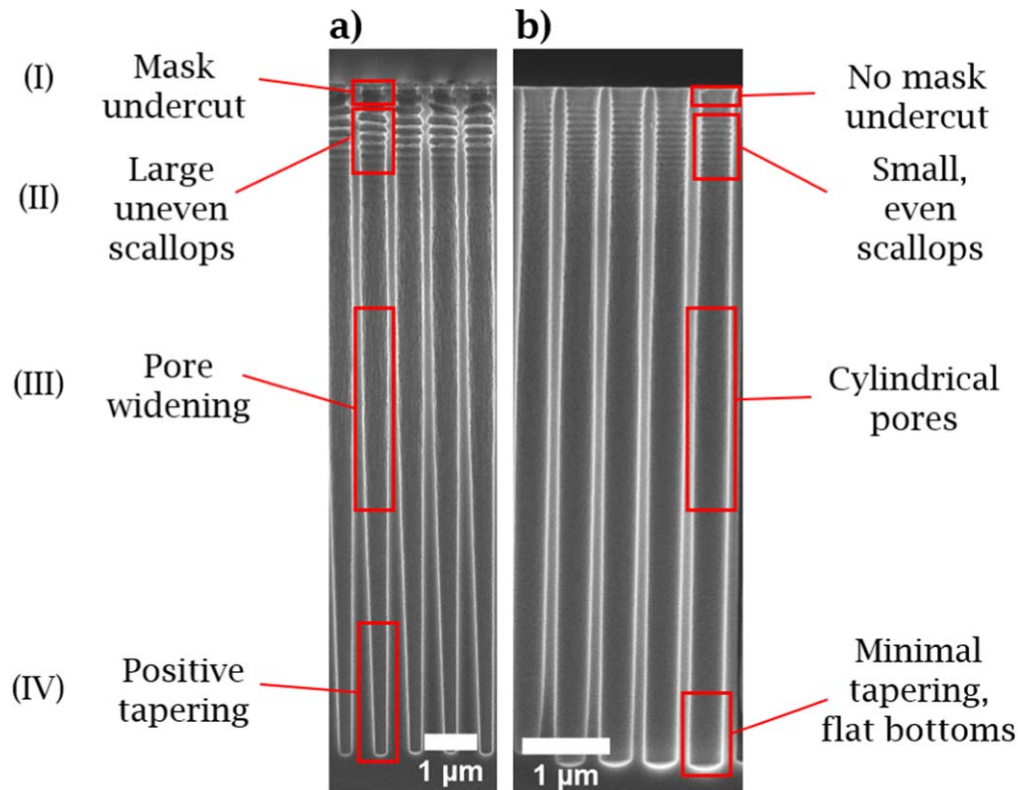


Figure 4. (a) SEM image of pores with a $d = 360$ nm mask diameter measured after etching by SEM showing the starting etch of this project based on the aspect ratio-optimised etching process of Grishina (page 72, table 4.5) [22]. (b) SEM image of pores with a $d = 360$ nm mask diameter measured after etching by SEM achieved with the final optimised etch. Exhibiting small, regular pores at the beginning, almost straight walls, flat bottoms and a high aspect ratio.

3. Results and discussion

3.1. Overview of initial and final results

To begin improving etching for photonic crystals, there must be an initial etch process on which to improve. The starting etch process, of which an example is shown in figure 4(a), was based on the one proposed by Grishina that was optimised to give the greatest aspect ratio [22]. While these etch parameters give an impressive aspect ratio up to $A = 40$, the profile of the pores exhibits a number of undesirable features. In short, (I) mask undercut, (II) large scallops, (III) abrasion of the centre of the pores and (IV) positive tapering.

- (I) As is apparent in figure 4(a), the large degree of mask undercut results in a greater pore diameter than desired, for instance, 480 nm pore diameter from a 360 nm mask diameter. The extent of the mask undercut can be graphically seen in the plot of nanopore diameter versus nanopore width in figure 5. While this increase in diameter could be compensated by reducing the pore size of the mask, this approach does not address the large, uneven scallops.
- (II) Controlling the first scallop gives control of all subsequent scallops. If the first scallop is large and underetched, then subsequent scallops will also have a greater diameter than desired. Thus control of scallops is closely linked to

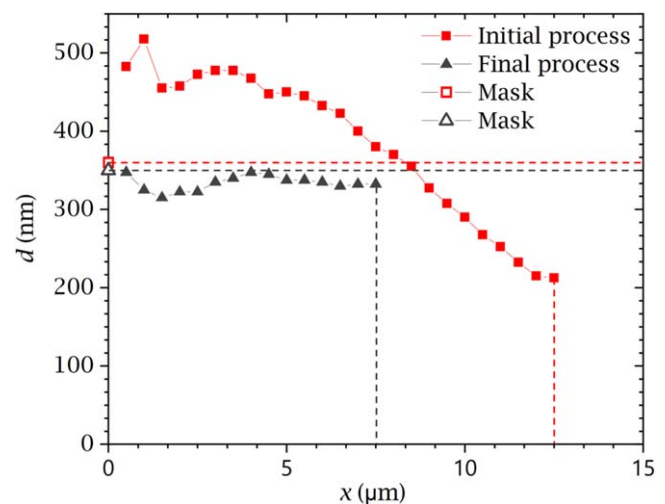


Figure 5. Diameter d in nm of a nanopore versus the depth x inside a nanopore in μm for the pores shown in figure 4. The graph demonstrates the difference in consistency and mask undercut between the starting etch (red squares), where the outlined square at $x = 0$ is the mask aperture diameter and the final optimised etch (grey triangles), where the outlined triangle at $x = 0$ is the mask aperture diameter. Horizontal dashed lines indicate the mask diameter and vertical dashed lines indicate the maximum pore depth x_{max} . Data are averaged from measurements taken from 4 different pores.

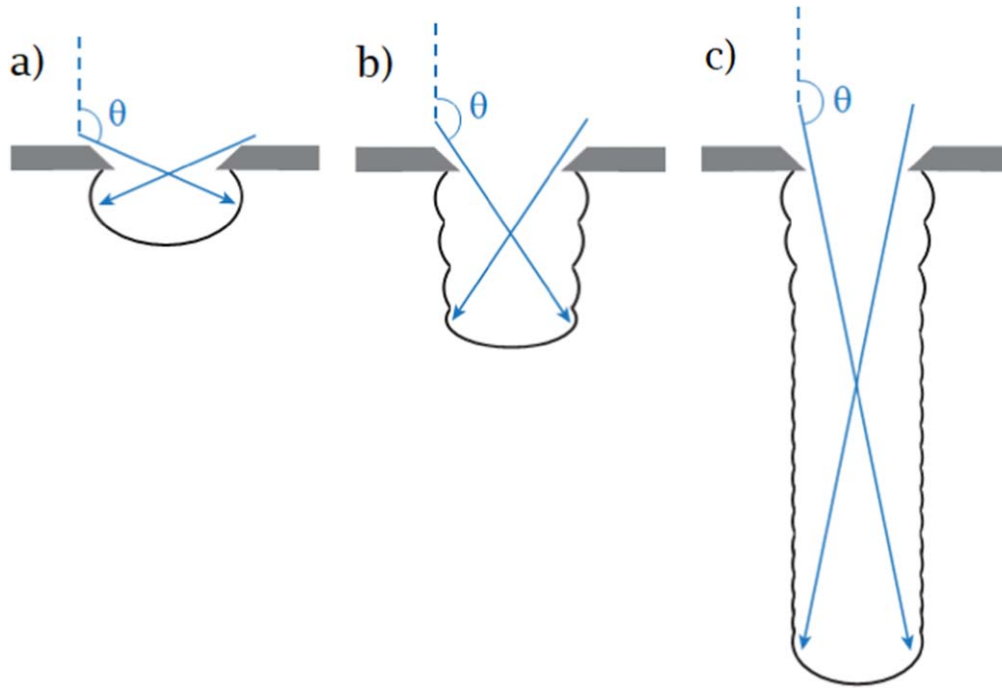


Figure 6. Cartoon illustrating the effects of angular distribution on the diameter of scallops at different points along the pore length. (a) Near the surface at the top of the pores, ions with a shallow angle to the surface (low θ) can access the walls of the pores, resulting in etching of the walls and widening of the pores. (b) Further down the pores, the ions with low θ can only reach the protective fluorocarbon layer at the top of the pore, so do not contribute to etching, whilst ions with higher θ continue to etch the bottom of the pores. (c) At high aspect ratio, at the bottom of the pores, only ions with very high θ can reach the unprotected end of the pore, resulting in a very directional etch.

minimizing mask undercut. Controlling the scallops will also create a smoother and more cylindrical pore, which is desirable for photonic crystal applications.

- III) The middle section of the nanopores has a rough appearance on the SEM image. This rough appearance is the beginning of the pore walls etching away. This becomes apparent as pore widening in nanopores with a diameter of 320 nm or less, which causes inconsistencies across the photonic crystal. This can greatly reduce the reflectivity of the photonic crystal and cause large shifts of the photonic band gap across the crystal [17]. In structures with a small pitch, which is required for photonic crystal devices operating in the telecommunications range, pore widening can even cause the breakdown of the walls between the nanopores, effectively destroying the structures, as was observed by Grishina *et al* [27].
- (IV) The initial etch process also exhibits significant positive tapering, narrowing of the bottom of the nanopores as shown in figure 5. This creates inconsistencies and a reduction in quality of the optical properties, similar to pore widening.

The final, optimised etch is shown in figure 4(b). There is no mask undercut, with the pore having the same diameter as the mask. The initial scallops are shorter and more even in shape. The pore walls are almost straight and there is no tapering, with only a 20 nm (or <6%) variation along the length of the whole pore, as shown in figure 5. The bottoms of the pores

are flat, which suggests that the etch process could be extended if required. The final etch depth is here shorter than the initial etch, $x_{\max} = 7.3 \mu\text{m}$ down from $x_{\max} = 12.5 \mu\text{m}$. As the 3D inverse woodpile photonic crystals of interest have a depth of $x_{\max} = 7.7 \mu\text{m}$ [17], which is much greater than the characteristic Bragg length of $0.3 \mu\text{m}$ [28], even the reduced depth is plenty sufficient for the desired application, with a majority of the length of the crystal etched. The final etch is much closer to the desired perfect cylinder and suitable for photonic crystal applications.

In the remainder of this work, each undesirable feature is addressed in turn, starting with mask undercut and large scallops, followed by pore widening and finally tapering. The parameter changes which successfully reduced the problems are described. Many parameter changes effect multiple featured and are referred in several sections.

3.2. Mask undercut and scallops

While mask undercut and scallops may appear to be two separate issues, they are integrally linked. Mask undercut is caused by the quasi-isotropic nature of the etch step, most importantly in the first few etch cycles which form the most pronounced scallops. The initial 5 to 10 scallops are often much wider and longer than subsequent scallops. The increased width is due to the effective angular distribution of the ions which decreases with nanopore depth. As is shown in figure 6(a), early on after a few etch steps when the nanopore

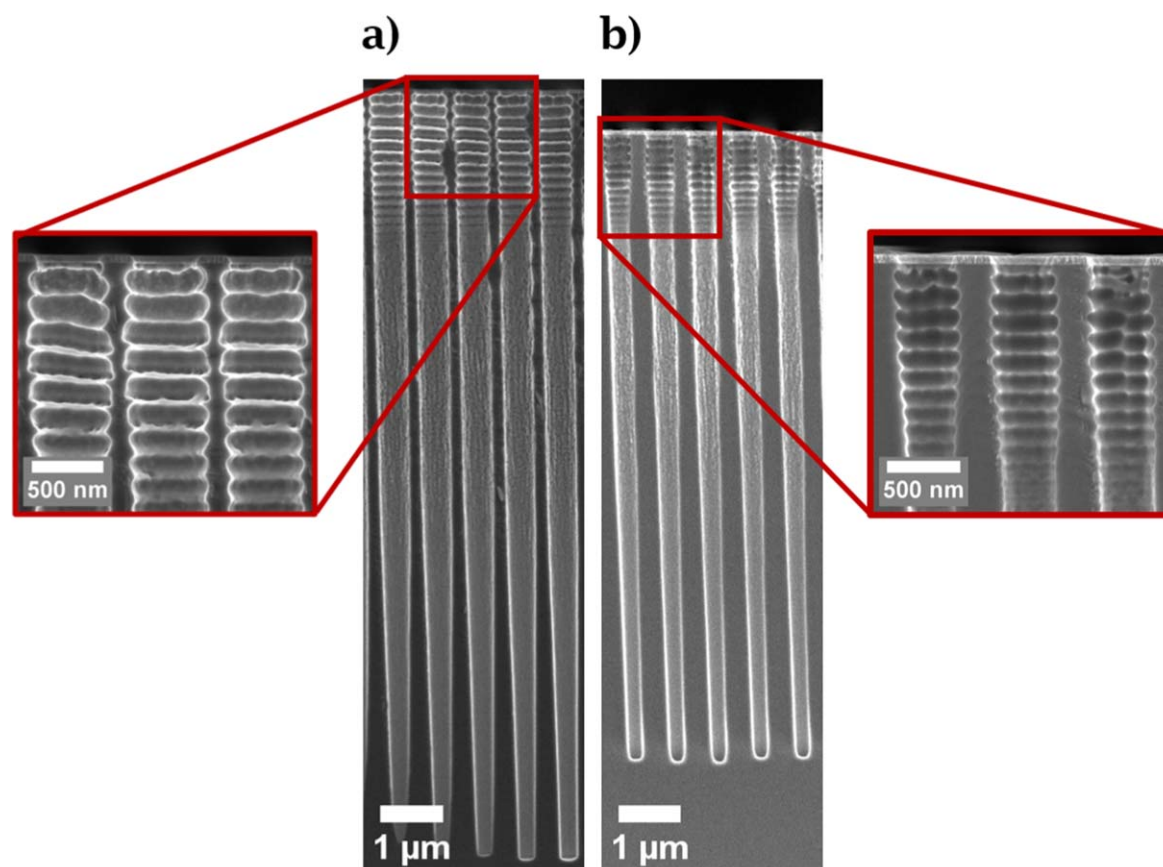


Figure 7. SEM images of pores with a 450 nm mask diameter showing the effects of varying the etch step time in a 2-step process with 160 cycles. (a) 3 s etch step time and (b) 2 s to 3 s etch step time ramp. Red boxes provide higher magnification images of the tops of the nanopores to help illustrate the changes in mask undercut and scallop width. The degree of mask undercut and scallop width is reduced upon shortening of the initial etch step time.

is shallow, ions with a broad angular range θ , can readily access the exposed silicon wall which results in lateral etching to form the early scallops. After more and more steps, see figures 6(b), (c), the walls at the top of the nanopore are protected by fluorocarbon and the deeper, exposed silicon walls are only accessible by ions with an increasingly narrow angular range θ . This reduction in angles with depth also affects the F radicals, which have no directionality and are a significant part of the plasma, though at higher pressures radical–radical collisions within the pore will increase the angular range of the etching radicals. The length of the scallops is related to the number of reactive species, ion and radicals, that are available to etch during an etch step. The decrease in scallop length with increasing nanopore length is due to the decreasing number of available species for etching in deep pores. Firstly, ions and radicals traveling at oblique angles with respect to the surface, that is, more oblique than the critical angle θ for a particular depth (as shown in figure 6), will be lost to the side walls [21]. Secondly the influence of image force becomes more prominent as the nanopore lengthens as the ions must successfully pass a longer silicon wall before reaching the exposed silicon bottom to etch. Thirdly, only ions with sufficient energy from the whole energy distribution can reach the end of a longer pore

with enough energy to remove the protective fluorocarbon layer and continue the etching process.

To reduce the width of the first scallops, and thus the mask undercut, the angular distribution of the reactive species or the number of etching species must be reduced by the following set of parameters. Reducing the pressure increases the mean free path of the ions and thus reduces the angular distribution $\Delta\theta$. To reduce the length of the first scallops, the number of etching species in the first etch steps must be reduced. The number of etching species is affected by the etch step time and the pressure. In addition, the capacitively coupled plasma (CCP) power also affects the energy of the ions and their ability for remove fluorocarbon from the bottom of the pores. A high CCP power results in more ions with sufficient energy to reach the bottom of the pore and remove the fluorocarbon to continue the etching process, but a too high CCP power in the early etch steps increases mask undercut and scallop size by contributing to removal of fluorocarbon from the walls by ions with a shallow angle. The effects of these parameters are further explored in the following subsections.

3.2.1. Etch cycle time. To reduce the mask undercut and size of the scallops the first parameter we varied the initial etch

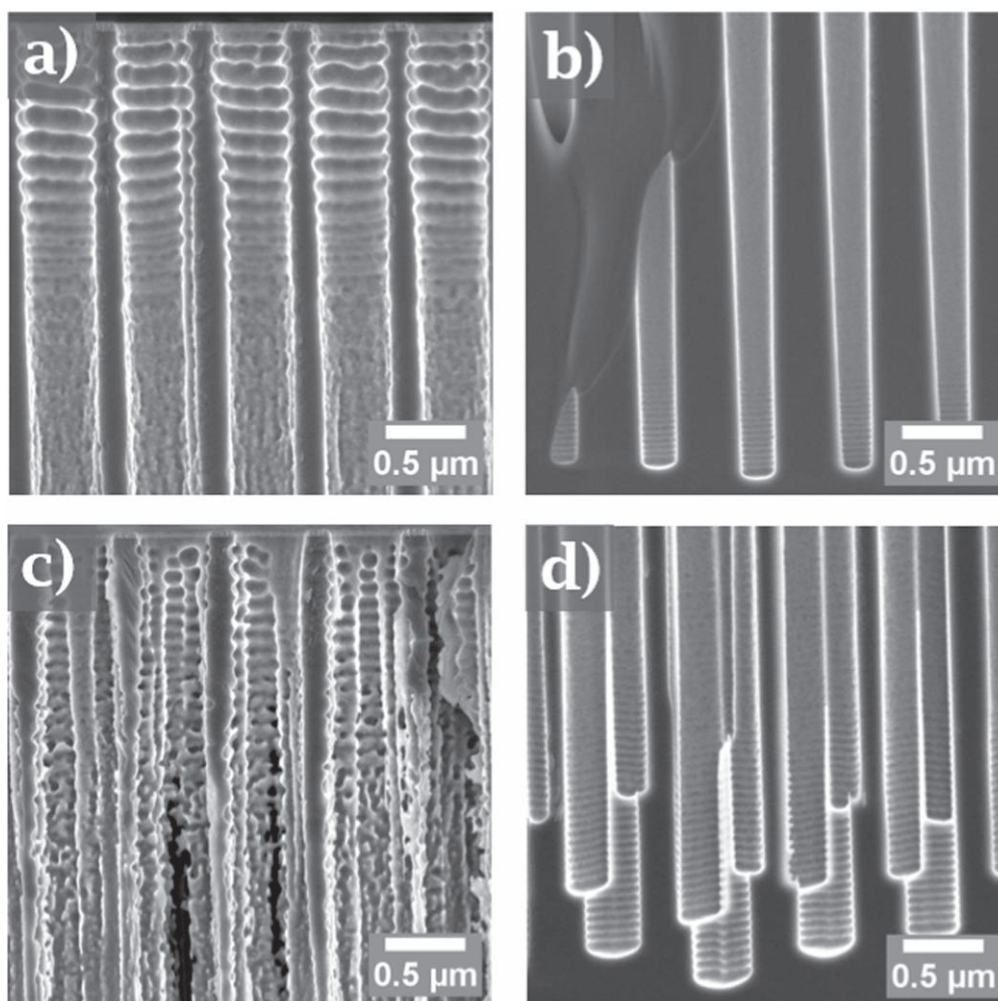


Figure 8. SEM images of pores with a 450 nm mask diameter showing the effects of extreme variations in etch cycle time in a 2-step process with 200 cycles. (a) and (b) 2 s to 3 s etch step ramp, (c) and (d) 1.5 s to 4 s etch step ramp, showing in (a) the beginnings of the silicon wall breaking down with increase etch time and in (b) the pore splitting occurring when the initial etch cycle time is too low.

step time t_i , which was reduced from $t_i = 3$ s to 2 s. To maintain the depth of the pores and to reduce the positive tapering, the etch step time was ramped from $t_i = 2$ s and ending with final etch step time $t_f = 3$ s. In figure 7 the effects of changing from a 3 s etch step time (Figure 7(a)) to a ramp from 2 to 3 s (figure 7(b)) are shown. The depth of the pore is reduced, from 13.8 to 11.3 μm with the 2 to 3 s etch step time ramp since the effective etch time has decreased. If desired, this depth can be compensated by increasing the number of cycles or extending the etch cycle end time. With a mask aperture of 450 nm, the 3 second etch gives a larger pore diameter of 550 nm (Figure 7(a)), while the 2 to 3 s etch gives a pore diameter of 440 nm (figure 7(b)). Reducing t_i from 3 to 2 s has effectively removed the mask undercut and scallop width, resulting in a pore with the same diameter as the mask. Changing from 3 to 2 to 3 s etch step time ramp also reduces the length of the second scallop from 170 to 130 nm, a significant reduction in scallop length as desired.

As the pore becomes longer, the influence of image force increases and the angular range θ becomes narrower reducing the effective number of reactive species resulting in the etch

becoming slower. Increasing the etch step time as the nanopore length increases, should allow more reactive species to access the bottom of the pore, thus increasing the length. To this end, the t_f was increased beyond 3 s. Figure 8(a) shows the top of a set of nanopores with a 2 to 3 s ramped etch step time, exhibiting distinct scallops and minimal mask undercut. When t_f is increased to 4 s to give a 2 to 4 s ramped etch step time, the scallops lose definition, becoming uneven, the nanopores also become wider, see figure 8(c). When we further increase t_f to 5 s, parts of the silicon walls between the nanopores to begin to break down. Longer etch step time gives more time for removal of the protecting fluorocarbon from the walls before re-protection, causing the walls to become laterally etched. This means that one must always compromise between nanopore length, as longer nanopores require longer t_f , and the integrity of the walls of the nanopore.

In figure 8(b) the bottom of pores from an etch step time ramped from 2 to 3 s is shown. The pores end in a flat bottom, albeit with some positive tapering, though less than with the initial etch process in figure 4(a). Figure 8(d) shows the

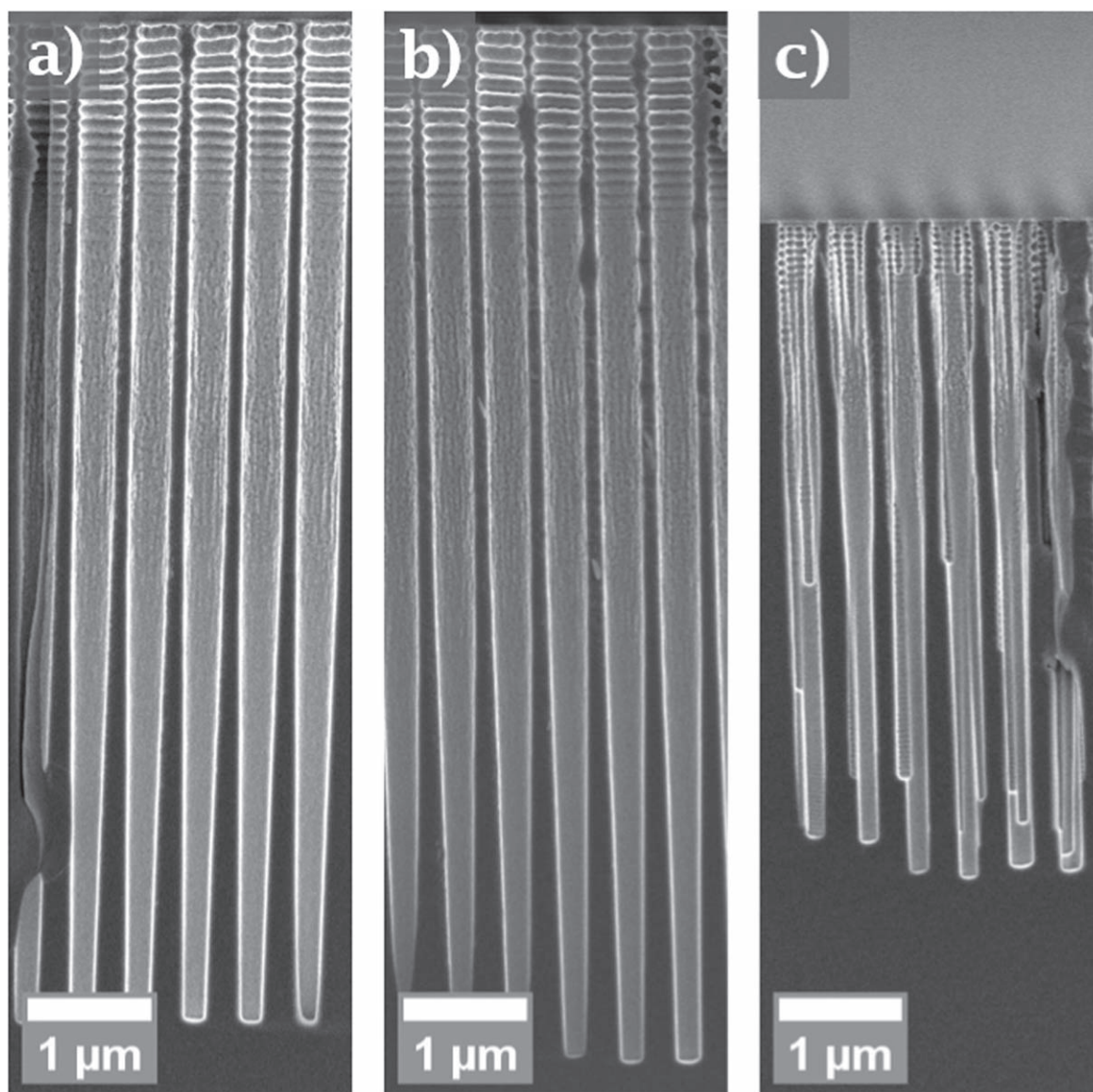


Figure 9. SEM images of pores with a 450 nm mask diameter showing the effects of CCP power in a 2-step process with 180 cycles. (a) 80 W to 90 W CCP power ramp (b) 60 W to 90 W power CCP ramp and (c) 50 W to 80 W CCP power ramp showing the pore splintering which occurs when the initial CCP power is too low.

effects of t_i being reduced to 1.5 s, resulting in an uneven etch with branching and pore tip splitting. These branches and splits form at various points along the pore, some starting at the top and others starting further down. Due to the nature of cleaving and SEM as an analytical technique, further analysis would be required to pinpoint where exactly all splits form, but this is beyond the scope of this current work. The shorter $t_i = 1.5$ s is too short to remove the fluorocarbon from the bottom of the pores, resulting in an uneven etch.

To conclude this subsection, reducing the initial etch time $t_i = 2$ s reduces the mask undercut and scallop width. Further reduction of the initial etch time t_i causes pore splintering. Longer t_f are required to prevent positive tapering. Increasing t_f to 4 s causes the walls of the pores to be etched, eventually resulting in complete breakdown of the pore walls.

3.2.2. Capacitively coupled plasma power. The Capacitively Coupled Plasma (CCP) is produced by applying a single radio frequency (RF) across the sample [29]. Since there is a potential difference between the plasma and the sample, there is a bias potential that effectively gives the sample a negative potential that accelerates the SF_5^+ ions towards it. The CCP power controls the energy of the ions hitting the substrate. A higher CCP power also assists in the removal of the fluorocarbon protecting layer and may also contribute to the removal of the protecting layer from the walls at higher pressures (>10 mtorr) which would lead to unwanted lateral etching. Figure 9 shows three samples to study the reduction of the CCP power in order to reduce the scallops in a 2-step etch cycle. There is no significant difference in the initial scallops, mask undercut nor depth

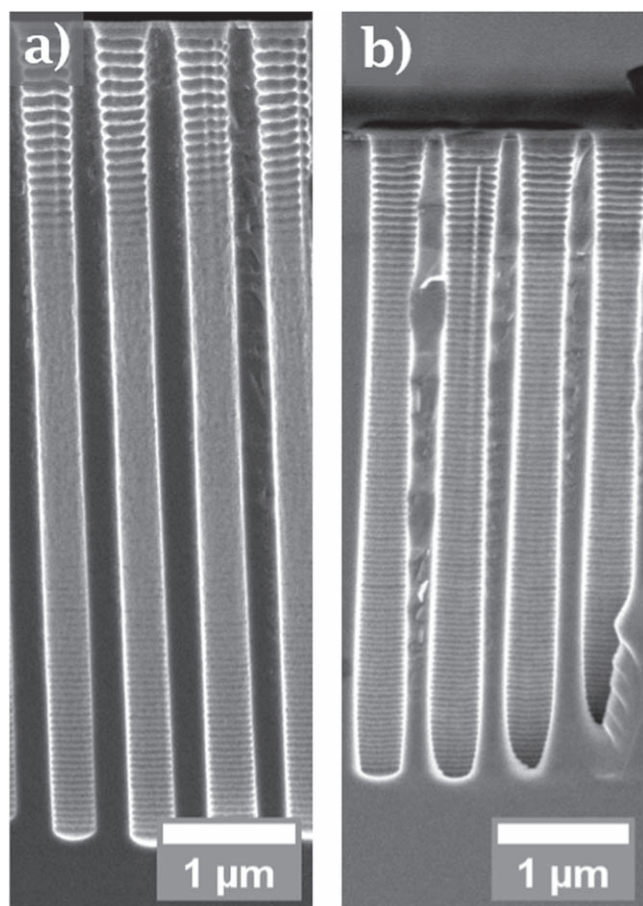


Figure 10. SEM images of pores with a 400 nm mask diameter showing the effects of etch cycle pressure in a 3-step process with 100 cycles. (a) 26 mtorr SF_6 pressure and (b) 15 mtorr to 26 mtorr SF_6 pressure ramp. The length and diameter of the initial scallops are reduced when the initial SF_6 pressure is reduced.

of the pore when changing the initial CCP power from 80 W (Figure 9(a)) down to 60 W (figure 9(b)), indicating that the ion energy is still sufficient at 60 W to fully remove the fluorocarbon at the bottom of the pore. With further reduction to 50 W a splitting of the pores was observed, as shown in figure 9(c). This is caused by an incomplete fluorocarbon removal resulting in an uneven etch, as was previously observed when etch time was reduced too far in figure 8(d). Since varying the CCP power made almost no change in the results of the etch for our system until it was so low that the fluorocarbon was not fully removed, it was concluded that maintaining a relatively high CCP power of 80–90 W and varying other parameters, such as etch time, gave better control over the scallops and mask undercut.

3.2.3. SF_6 etchant pressure. Reducing the pressure during the etch step slows down etch rate and increases directionality. Figure 10 shows the pores resulting from a 3-step process where the etch pressure was reduced from $p = 26$ mtorr in figure 10(a) to a 15 to 26 mtorr pressure ramp in figure 10(b). Reducing the pressure during the etch step results in a reduction in the length and width of the scallops.

The ratio of the narrowest to the widest point of the width of the 3rd scallop is 330:410 nm at 26 mtorr and 360:400 nm for 13 mtorr, in other words a significantly smaller scallops. The length of the third scallop is reduced from 90 nm at 26 mtorr to 60 nm at 13 mtorr. This shows that reducing the initial amount SF_6 in the etch step is an effective way to create small scallops.

To reduce positive tapering which would result from the decreased number of reactive species, we decided to increase the pressure at the end of the whole etch process. In figure 10(b) the beginnings of a negative taper, widening at the bottom of the pore, is apparent, indicating that 26 mtorr is more than required to eliminate positive tapering. This negative tapering suggests that end pressure is an effective way to control both the tapering of the nanopore as well as the initial scallops.

To summarise this subsection, reducing the start pressure of the SF_6 in the etch step decreases the size the first scallops, reduces the relative width and the length of the scallops. Increasing the end pressure is an effective method to eliminate positive tapering, with a high pressure causing a negative tapering.

3.2.4. SF_6 etchant flow. In a 3-step process the etch step is split into a boost step and an etch step. In addition to reducing the pressure of the etch step, it is also possible to reduce the pressure of the boost step. The pressure is at a set value for both the boost and etch steps, though as the etch step the throttle is controlled by the machine to maintain a pressure value, changing the SF_6 flow does not change the pressure of the etch step, only the boost step. The boost step is at 100% throttle, meaning that the valve to the vacuum pump is fully open though no pressure value is recorded by the machine. This results in as low as possible pressure at a given SF_6 flow rate, giving a low angular ion distribution and high ion energy. The gas flow of the SF_6 can be reduced and as the pressure control remains at 100% throttle, the pressure is effectively reduced during the boost step. The effects of reducing the SF_6 flow from 65 to 50 sccm are shown in figure 11. Reducing the SF_6 gas flow to less than 60 sccm results in incomplete removal of the fluorocarbon during the boost step as seen in figure 11(b). The incomplete removal results in a nanopore diameter smaller than that of the mask and a large amount positive tapering early on in the nanopore, giving the nanopores an undesired funnel-shaped appearance. This is a different result than in the 2-step process, where pore splintering was found (figures 8(d) and 9(b)). This suggests that the 3-step process results in an even removal of fluorocarbon, starting at the center of the nanopore, while the 2-step process gives a random removal across the diameter of the nanopore. There is no significant reduction in the size of the scallops when the SF_6 flow is reduced.

To conclude this subsection, reducing the SF_6 flow, and thus pressure of the boost step, did not improve the etch for our application. When the SF_6 flow is reduced too far, for

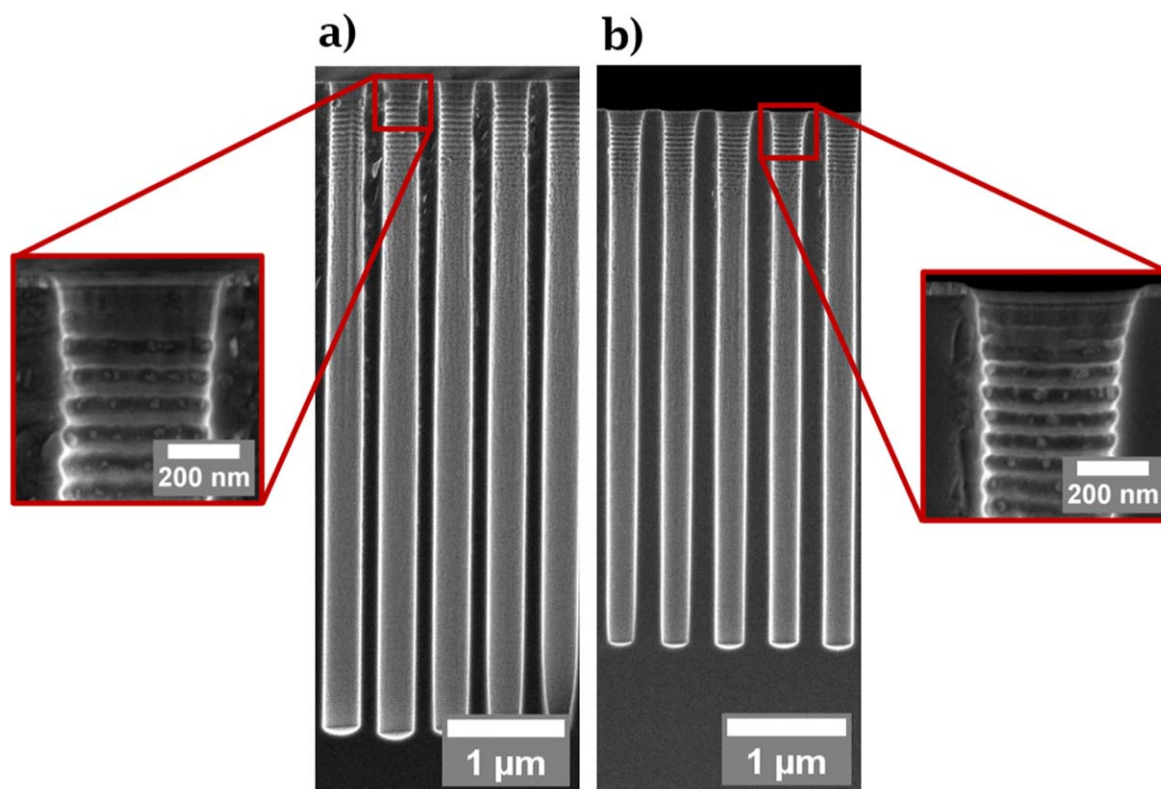


Figure 11. SEM images of pores with a 450 nm mask diameter showing the effects of SF_6 flow in a 3-step process with 180 cycles. These images show a reduction in negative tapering with a reduction of SF_6 flow. (a) 65 sccm and (b) 50 sccm. The diameter of the pore is decreased when the SF_6 pressure is reduced to 50 sccm, giving the pores a ‘funnel-like’ profile. Red boxes provide a higher magnification image of the the tops of the pores to further highlight the difference in form at the start of the pore.

example 50 sccm, the fluorocarbon removal is not complete, resulting in a reduction in pore diameter. In applications where there is still issues with mask undercut which cannot be fixed by reducing the initial etch step time, SF_6 flow may be a useful tool for for controlling the diameters of nanopores.

3.3. Pore widening

Pore widening occurs in the middle section of the length of the nanopore as shown in figure 4(a) and 5, and may occur in nanopores with no mask undercut or tapering. Figure 12 shown an example of pore widening in a sample created using a 2-step process. The sample has no mask undercut and a small amount of positive tapering, only the diameter at the middle of the nanopores is larger than the mask diameter. In wider nanopores, for example 500 nm diameter, this phenomenon manifests mainly as a rough appearance in the middle section of the pore as is highlighted in figure 4(a). In smaller diameter nanopores, for example the 280 nm nanopores in figure 12, this roughness becomes a widening of the middle section of the pores to a diameter greater than that of the mask. This roughness and widening only affects the middle section of the nanopore. In all cases observed throughout this study, the scallops are visible at the bottom of the pore and often the diameter has returned to that of the mask or even smaller. In an attempt to elucidate when in the etch process this roughness begins to form, the cycle number

was incrementally reduced from $N = 200$, where the roughness begins after 10 to 12 scallops, to $N = 50$. Even by $N = 50$ cycles, after 10 to 12 scallops the roughness obscures the scallops. This suggests that the roughness is not just an artifact caused by the long etch times required to create high aspect ratio structures, but occurs relatively early on in the etching process.

Widening in the middle length of a pore is caused by the balance between ion energy and image force. The positively charges ions continually lose energy as they travel along the negatively charged wall. At some point, which is defined by the energy of the ions and the diameter of the nanopore, the ions will have lost so much energy that they are pulled to the wall by the image force and hence they begin to laterally remove the protecting fluorocarbon layer, exposing the Si wall to the quasi-isotropic etch of the fluorine radicals. As the neutral etching species, such as radicals, are not affected by image force and are the majority component of the plasma, after the loss of ions which caused the pore widening the etch continues unperturbed by image force effects.

We found that no parameter change in the 2-step Bosch process could remove, or even significantly reduce the pore widening. To obtain more control over the etching process was the main motivation to move from a 2-step to a 3-step Bosch process. For the boost step, the throttle was set to 100%, meaning that the valve to the vacuum pump was

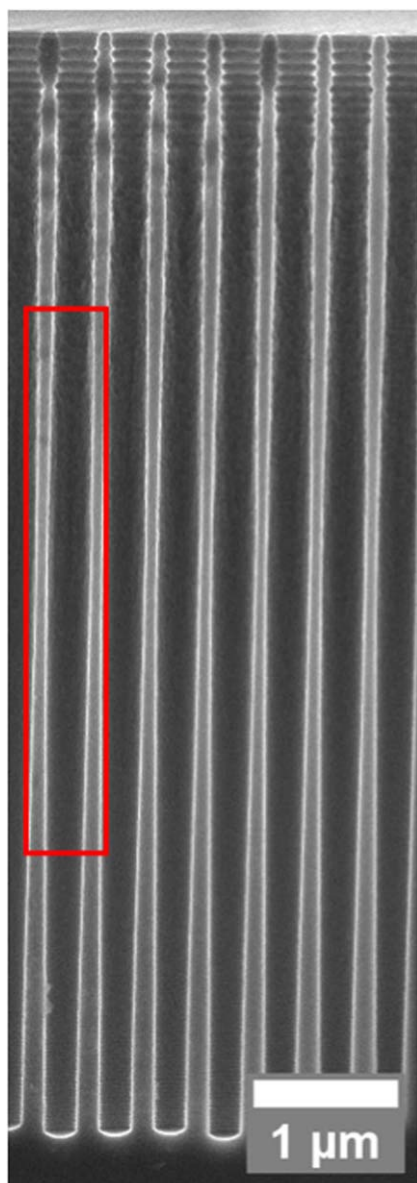


Figure 12. SEM images of pores with a 280 nm mask diameter showing widening half way down the pore length in a 2-step etch process with 200 cycles. The pore widening is highlighted by the red box.

opened fully. This gives the lowest possible pressure, which is not recorded by the machine, with the given gas flow of 65 sccm (see section 3.2.4). The pressure was returned to $p = 26$ mtorr for the etch step. The difference when changing from a 2- to 3-step process is shown in figure 13. The 2-step process exhibits roughness of the walls from about a third of the length until two thirds of the length, which obscures the scallops. In the 3-step nanopores, the scallops can be observed over the whole length of the nanopore, indicating that the 3-step process offers much more control thus giving a consistent etch for the whole length, as desired from the outset. At the low pressure used in the boost step, the number of ion collisions in the plasma are reduced. This narrows the ion angular distribution and decreases the loss of ion energy

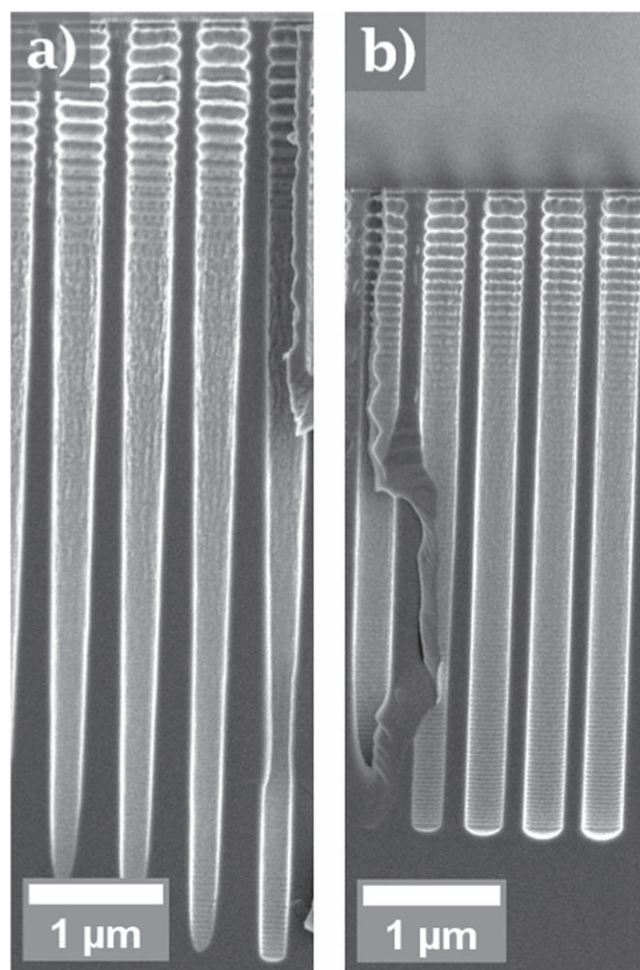


Figure 13. SEM images of pores with a 400 nm mask diameter showing the effects of changing from (a) a 2-step etch process to (b) a 3-step etch process over 100 cycles. Moving from a 2- to 3-step process results in a reduction in pore widening, mask undercut, positive tapering but also length.

through collision, effectively increasing the ion energy at constant depth. Increased ion energy reduces the number of ions lost to the walls to image force and thus reduces the pore widening.

Although our goal was to reduce the pore widening, changing to a 3-step process also affects other properties of the nanopores. The 3-step process results in shorter nanopores than the 2-step process. This is because both etches used a 3 s etch step and in the 3-step process, 1 s out of 3 was used for the low pressure boost step. At low pressure the etch speed is reduced due to the lower concentration of reactive species. The 3-step process shows a very straight walled profile whilst the 2-step process has a significant positive tapering, even by the same length as the shorter 3-step etched pores. The size of the initial scallops was also reduced when moving to a 3-step process. The reduction in pressure during the boost step increases directionality of the etch and also reduces the speed of the etch, giving a reduction in the width and length of the first scallops. The second scallop of the 2-step process has a width of 530 nm and a length of 170 nm and the second

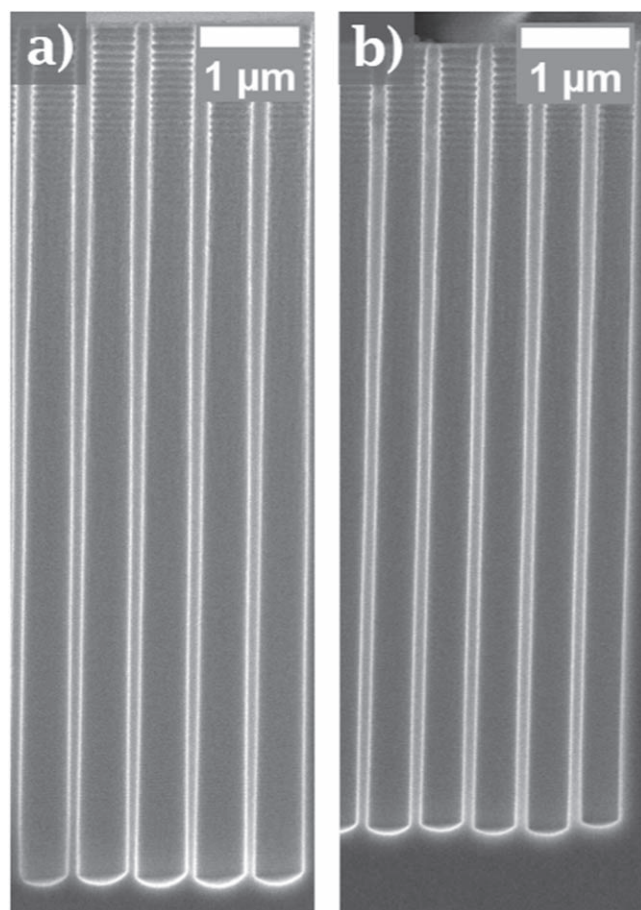


Figure 14. SEM images of pores with a 400 nm mask diameter demonstrating a reduction in negative taper when the boost step time is varied in an etch with a 2 s to 4 s etch cycle time ramp over 180 cycles. (a) 1 s to 2 s boost step time ramp, showing negative tapering and (b) 1 s to 3 s boost step time ramp, with no negative tapering.

scallop of the 3-step process has a width of 470 nm and a length of 130 nm. From visible inspection, the scallops of the 3-step process appear more uniform and even, with the scallops of the 2-step process often having wavy or curved bottoms. This arises from the decoupling of the fluorocarbon removal and silicon etch steps; in the 2-step process as soon as the fluorocarbon is removed, the etch begins. If the fluorocarbon is removed unevenly then the etch will be uneven. In a 3-step all fluorocarbon is removed before the etching begins, regardless of how even the removal is, allowing for an even, uniform etch.

To summarise this subsection, moving from a 2-step to a 3-step process results in a reduction of the pore widening as was aimed for. As a bonus, other unwanted features such as mask undercut, large scallops and positive taper were also reduced. On the downside, the nanopore depth was reduced. While this reduction can be regained by adding more cycles, this does significantly lengthen the etch time and require the number of cycles to again be optimised for this new process. Moreover, the already achieved nanopore depths are sufficient for our subsequent 3D photonic crystal fabrication, see the work of van der Broek *et al* [30].

3.4. Tapering

Tapering is the increasing or decreasing of the nanopore diameter with depth. In this work a reduction of nanopore diameter with length, positive tapering, was much more common than negative tapering. This is due to our desire to have high aspect ratio pores. The longer the nanopores become, the greater the risk of positive tapering. Due to loss of ions through image force, the number of ions reaching the bottom of the pore to etch is reduced as nanopore length increases, resulting in a positive taper and eventually an end to the etch process. Examples of positive tapering are shown in figures 4(a), 7 and 13 which also give clear examples of eliminating positive tapering, at the expense of the maximum nanopore depth.

To mitigate positive tapering it is necessary to increase parameters to increase the isotropy at the end of the etch. This is achieved by increasing by increasing the amount of reactive species later in the etch process via the pressure or by increasing the etch cycle time. By definition, to remove the positive taper any change will increase the isotropy of the etch and contribute to side wall erosion as in figure 8(c) when the end etch cycle time was increased to t_f 4 s.

The examples of negative tapering, or widening of the bottom of the nanopores, found in the course of this work have been few, though negative taper was briefly mentioned in section 3.2.3. An example of negative taper is shown in figure 14. In this case the effects of varying the length of the boost step was investigated. A 2 to 4 s etch step time was used and the boost step time was increased from a 1 to 2 s ramp in figure 14(a) to 1 to 3 s ramp in figure 14(b).

As all time ramps are linear, a boost step of 1 to 3 s on an etch step of 2 to 4 s effectively means that the etch time remains constant at 1 s. Lengthening the boost step ensures full fluorocarbon removal for the whole depth of the nanopore and the etch step proceeds for 1 s at all cycles in the etch. As these conditions give a very straight pore profile, it seems that enough reactive species reach the bottom of the pore even at full depth, hence 1 s is sufficient for etching after the removal of fluorocarbon.

On the other hand, a 1 to 2 s boost step on a 2 to 4 s etch cycle (figure 14(b)), results in the end of the etch having both a longer removal and etch steps. Judging from the lack of positive taper or pore tip splitting, the boost step was adequate to remove the fluorocarbon. The etch cycle time was however longer than necessary, with the long etch time resulting in greater lateral etch. As each cycle etches a little further out, this manifests as negative tapering.

In summary of this subsection, positive taper is often a compromise between the taper, length and pore widening. The 3-step process gives more control over the tapering than the 2-step. Increasing the pressure is also method to eliminate positive tapering, though may affect the integrity of the walls. Negative tapering is rarer in this

work, but can result from a too high end pressure or a too short boost step time to etch step time ratio at the end of the etch. Tapering can be controlled by carefully ramping the mentioned parameters to find a balance between length, side wall erosion and tapering. Tapering is the prime example of RIE being a technique of balance and compromise.

4. Conclusion and outlook

In this work, an etching process is studied and optimized to etch cylindrical nanopores in silicon, with a diameter in the range between 280 and 500 nm and a depth around 7 μm , corresponding to high depth-to-diameter aspect ratios between 14 and 25. Such samples are very well suited for the realization of nanostructures for silicon nanophotonics.

The remaining deviations from a perfect cylinder are within tolerances [17] to create photonic crystals with high reflectance and a well defined photonic band gap. The somewhat shorter length is remains sufficient for our applications and may be further improved by increasing the number cycles, although doing so would require further optimisation. The current optimisation has been achieved by manipulation of multiple etch parameters and moving from a 2-step process to a 3-step DREM Bosch process. In future work the 3-step process could be further improved by the use of a gas which is chemically inert with respect to silicon, such as argon, to ensure removal of the fluorocarbon but no chemical etching of the silicon, thus truly decoupling the removal

and etch steps. The ability to exponentially ramp parameters, instead of linearly, would also give more freedom. We foresee that moving to a 4-step DREAM (deposit, remove, etch, ash, multistep) process [19] with added oxygen plasma step to further protect the walls by formation of a silicon oxide layer, may also offer more avenues of to improve and expand the RIE of nanostructures even further.

Acknowledgments

We acknowledge support from NWO-TTW Perspectief program P15-36 'Free form scattering optics' (FFSO).

Data availability statement

The data that support the findings of this study are openly available at the following URL/DOI: <https://doi.org/https://zenodo.org/record/7293051#.Y8k7EXbMJPZ>.

Appendix

Here in table 2 is a full list off all parameters used in the etch processes presented in this work. The figure numbers refer to which figure image in the main text the parameters relate to.

Table 2. Etch parameters of the etch experiments relating to the SEM image. The columns refer to figures as given at the top.

Parameter	Unit/figure	4a	4b	7a	7b	8a/b	8c	8d	9a	9b	9c	10a	10b	11a	11b	12	13a	13b	14a	14b
Cycles	Number	160	180	160	160	160	160	160	160	160	180	100	100	180	180	200	100	100	180	180
Deposition time	Seconds	1.6	1.6	1.6	1.6	1.6	1.6	1.6	1.6	1.6	1.6	1.6	1.6	1.6	1.6	1.6	1.6	1.6	1.6	1.6
Etch time	Seconds	3.0	2.0	3.0	2.0	2.0	1.5	1.5	3	3	1.8	1.8	1.8	2.0	2.0	2.0	3	3	2.0-4.0	2.0-4.0
			to 3.8		to 3.0	to 3.0	to 4.0	to 3.0			to 3.5	to 2.7	to 2.8	to 3.8	to 3.8	to 3.0				
Deposition pressure	mtorr	20	20	20	20	20	20	20	20	20	20	20	20	20	20	20	20	20	20	20
Etch pressure	mtorr	26	13 to 22	26	26	26	26	26	26	26	26	26	15 to 26	13 to 22	13 to 22	13 to 26	26	26	26	26
SF ₆ flow	scm	65	65	65	65	65	65	65	65	65	65	65	65	65	50	65	65	65	65	65
C ₄ F ₈ flow	scm	200	200	200	200	200	200	200	200	200	200	200	200	200	200	200	200	200	200	200
ICP frequency	MHz	13.56	13.56	13.56	13.56	13.56	13.56	13.56	13.56	13.56	13.56	13.56	13.56	13.56	13.56	13.56	13.56	13.56	13.56	13.56
ICP power	Watts	1500	1500	1500	1500	1500	1500	1500	1500	1500	1500	1500	1500	1500	1500	1500	1500	1500	1500	1500
deposition																				
ICP power etch	Watts	1500	1500	1500	1500	1500	1500	1500	1500	1500	1500	1500	1500	1500	1500	1500	1500	1500	1500	1500
CCP frequency	KHz	380	380	380	380	380	380	380	380	380	380	380	380	380	380	380	380	380	380	380
CCP power	Watts	0	0	0	0	0	0	0	0	0	0	0	0	0	0	0	0	0	0	0
deposition																				
CCP power etch	Watts	70 to 80	70 to 90	70 to 80	70 to 80	70 to 80	70 to 80	70 to 80	80 to 90	60 to 90	50 to 80	70 to 80	70 to 80	70 to 90	80 to 90	70 to 80	60 to 90	60 to 90	70 to 80	70 to 90
Temperature	°C	10	10	10	10	10	10	10	10	10	10	10	10	10	10	10	10	10	10	10
Boost step time	Seconds	0	1.0 to 3.0	0	0	0	0	0	0	0	0	1.0	1.0	1.0 to 3.0	1.0 to 2.8	0	0	1.0	1 to 3	1 to 2
Boost throttle	Percentage	-	100	-	-	-	-	-	-	-	-	100	100	100	100	-	-	100	100	100

ORCID iDs

Melissa J Goodwin  <https://orcid.org/0000-0002-2803-9789>

Cornelis A M Harteveld  <https://orcid.org/0000-0002-6108-7985>

Willem L Vos  <https://orcid.org/0000-0003-3066-859X>

References

- [1] Kuiper S, de Boer M, van Rijn C, Nijdam W, Krijnen G and Elwenspoek M 2000 *J. Micromech. Microeng.* **10** 171
- [2] Balderas-Valadez R F, Agarwal V and Pacholski C 2016 *RSC Adv.* **6** 21430
- [3] Ezoe Y, Koshiishi K, Mita M, Mitsuda K, Hoshino A, Ishisaki Y, Yang Z, Takano T and Maeda R 2006 *Appl. Opt.* **45** 8932
- [4] Dubey R S and Gautam D K 2011 *Superlattices Microstruct.* **50** 269
- [5] Birner A, Wehrspohn R B, Gösele U M and Busch K 2001 *Adv. Mater.* **13** 377
- [6] Woldering L A, Tjerkstra R W, Jansen H V, Setija I D and Vos W L 2008 *Nanotechnology* **19** 145304
- [7] Ishizaki K, Suzuki K and Noda S 2016 *Photonics* **3** 36
- [8] Laermer F and Urban A 2019 *Plasma Process. Polym.* **16** 1800207
- [9] Wu B, Kumar A and Pamorthy S 2010 *J. Appl. Phys.* **108** 051101
- [10] Esashi M and Ono T 2005 *J. Phys. D: Appl. Phys.* **38** R223
- [11] Huff M 2021 *Micromachines* **12** 991
- [12] Guo H, Cao S, Li L and Zhang X 2022 *Mater. Sci. Semicond. Process.* **137** 106182
- [13] Ramaswami R 2002 *IEEE Commun. Mag.* **40** 138
- [14] Vos W L and Woldering L A 2015 Cavity quantum electrodynamics with three-dimensional photonic bandgap crystals *Light Localisation and Lasing* ed M Ghulinyan and L Pavesi (Cambridge: Cambridge Univ. Press) pp 180–216
- [15] Huisman S R, Nair R V, Hartsuiker A, Woldering L A, Mosk A P and Vos W L 2012 *Phys. Rev. Lett.* **108** 083901
- [16] Uppu R, Adhikary M, Harteveld C A M and Vos W L 2021 *Phys. Rev. Lett.* **126** 177402
- [17] Woldering L A, Mosk A P, Tjerkstra R W and Vos W L 2009 *J. Appl. Phys.* **105** 093108
- [18] Laermer F and Schilp A 1994 Method of anisotropically etching silicon US Patent 5501893A
- [19] Chang B, Leussink P, Jensen F, Hübner J and Jansen H 2018 *Microelectron. Eng.* **191** 77
- [20] Jansen H, Gardeniers H, de Boer M, Elwenspoek M and Fluitman J 1996 *J. Micromech. Microeng.* **6** 14
- [21] Jansen H, de Boer M, Wiegerink R, Tas N, Smulders E, Neagu C and Elwenspoek M 1997 *Microelectron. Eng.* **35** 45
- [22] Grishina D A 2017 3D silicon nanophotonics *PhD Thesis* University of Twente
- [23] Adhikary M, Uppu R, Harteveld C A M, Grishina D A and Vos W L 2020 *Opt. Express* **28** 2683
- [24] Woldering L A 2008 Fabrication of photonic crystals and nanocavities *PhD Thesis* University of Twente
- [25] Karttunen J, Kiihamaki J and Franssila S 2000 Loading effects in deep silicon etching *Micromachining and Microfabrication Process Technology VI* 4174, **90–7**
- [26] Gottscho R A, Jurgensen C W and Vitkavage D J 1992 *J. Vac. Sci. Technol. B* **10** 2133
- [27] Grishina D A, Harteveld C A M, Pacureanu A, Devashish D, Legendijk A, Cloetens P and Vos W L 2019 *ACS Nano* **13** 13932
- [28] Devashish D, Hasan S B, van der Vegt J J W and Vos W L 2017 *Phys. Rev. B* **95** 155141
- [29] Karouta F 2014 *J. Phys. D: Appl. Phys.* **47** 233501
- [30] van den Broek J M, Woldering L A, Tjerkstra R W, Segerink F B, Setija I D and Vos W L 2012 *Adv. Funct. Mater.* **22** 25